Application of Persistent Scatterer Interferometry for Land Subsidence Monitoring in Sydney, Australia using ENVISAT ASAR Data

A. H.-M Ng[a,*], L. Ge[a], K. Zhang[a], X. Li[a]

[a]Geodesy and Earth Observing Systems Group, The University of New South Wales, Sydney, Australia.

Abstract - The aim of this research is to investigate the terrain deformation in the metropolitan area of Sydney using multiple satellite radar imagery. The persistent scatterer interferometry (PSI) strategy developed at Geodesy and Earth Observing Systems Group (GEOS) of the University of New South Wales (UNSW) is used to map the land deformation in Sydney with C-band ENVISAT radar images in this study. A total of 49 ENVISAT images acquired from 21 April 2003 to 6 September 2010 over Sydney were used in this study. The results demonstrate that the area of Sydney was relatively stable with the majority of deformation at persistent scatter points within the range of -3 mm/yr to 3 mm/yr. The PSI result was overlaid with the water extraction bore and the boundary of Botany Sands Aquifer. No clear correlation between the groundwater extraction and the PSI measured deformation pattern has been observed.

Keywords: Urban, Radiometry, Space, Land, Radar Interferometry, Persistent Scatterer Interferometry

1. INTRODUCTION

There are many causes for land subsidence including groundwater extraction, high-rise building construction, underground tunnel excavation, and so on. Although land subsidence may not directly threaten human's life, these subsidence will lead to serious economic loss especially in urban area. Subsidence due to groundwater extraction is one of the major sources for the land subsidence in urban area throughout the world. Land subsidence in urban area can lead to serious problems. For example, it can lead to damage in buildings, roads, gas/water pipes, and even the telecommunication optical cables which causes the internet network disconnected. It can also lead to changes in elevation and slope of streams, canals and drains, affecting the rate of groundwater flow. Therefore subsidence mapping is essential to the understanding of the land as well as the management of urban area.

Spaceborne Radar Interferometry (InSAR) has shown its advantage in regional-scale subsidence measurement over the conventional methods such as GPS, levelling, total station, and extensometer due to several reasons: (1) it is less time consuming, (2) it is relatively easy to cover a large subsidence basin, (3) it requires less human power and (4) the cost is relatively lower than most conventional methods. It has been used for mapping land deformation in many applications, including volcanic activity (Yun et al. 2006), glacier movement (Goldstein and Werner 1998), crustal movement (Ge et al. 2009; Zhang et al. 2010) and underground mining activity (Ng et al. 2009). Persistent Scatterer Interferometry (PSI) is an extension of conventional InSAR techniques which allows for millimetre precision ground deformation mapping based on the utilisation of long time series of interferometric SAR image data, in order to improve the accuracy of the InSAR techniques. The first PSI algorithm, known as the 'permanent scatterers technique' (PSInSAR), was demonstrated by Ferretti et al. (2000) and Ferretti et al. (2001). PSInSAR addressed several issues of the InSAR technique including the atmospheric disturbances, temporal and spatial decorrelation and phase ambiguity resolution. Since the development of PSInSAR, several PSI algorithms have been developed by different researchers to improve the PSI techniques as well as to avoid the patent issue (around PSInSAR). All PSI techniques are based on the same basic estimation strategy. The GEOS-PSI estimation strategy used in this study, developed at Geodesy and Earth Observing Systems Group (GEOS) of the University of New South Wales (UNSW), are developed on the basis of the PSI techniques described by Ferretti et al. (2000, 2001) and Kampes (2006). The GEOS-PSI technique offers several improvements, including: (1) better determination of the reliability of the estimated point scatterer (and hence improved accuracy of the PS point identification as well as the estimated displacement); (2) maximising the pixel density in the PSI result (but preserving its accuracy). The objective of this study is to investigate the land subsidence in Sydney city, Australia using the GEOS-PSI estimation strategy to enhance the understanding of the subsidence processes.

2. STUDY AREA

Sydney city is in the Sydney Basin that is a sedimentary basin consisting of Permian and Triassic sedimentary rocks. Sydney's urban area covers approximately 1788km^2 with population of approximately 4 millions as at 2006. Sydney lies over three stratigraphic divisions: Narrabeen group, Hawkesbury sandstone and Wianammatta group (McDonald 2008).

Botany Sand Beds Aquifer, the biggest and oldest aquifer in Sydney region, is a costal sand bed aquifers which are readily recharged by direct rainfall permeation. It consists of Aeolian sand deposits that envelope Botany Bay and covers an area of 91.12 km^2. There are more than 600 bores in operation as at 2008. The Botany Sands Aquifer is a shallow aquifer system basin and is mainly unconfined (Jankowski and Beck 2000) where groundwater extraction in such area could lead to subsidence. In addition to Botany Sand Beds Aquifer, there are several alluvial aquifers located along the Sydney coastline, for example Double Bay, Rose Bay, Coogee, Collaroy and Manly, which are much smaller in size.

3. METHODOLOGY

A flow chart of the GEOS-PSI estimation strategy is shown in Figure 1. The single reference (master) image strategy (Ferretti et al. 2000, 2001) is used in GEOS-PSI to form the interferogram stack. This interferometric stacking strategy utilises all images in the image stack, including the pairs with large spatial baseline. The master image is selected with perpendicular baselines and temporal baselines as short as possible, and with Doppler centroid near the average Doppler centroid of all available SAR images in order to maximise the total coherence of the interferometric stack. Next, differential interferograms are generated between the master image and each slave image using the 2-pass DInSAR approach (Hanssen

2001; Massonnet et al. 1993). The spectral range and azimuth filtering, commonly used in the conventional InSAR processing, is not applied. The linear phase components of the orbital error in each interferogram can be estimated using an FFT and then removed from the interferogram. The non-linear parts will be included in atmospheric phase component and will eventually be removed in later process.

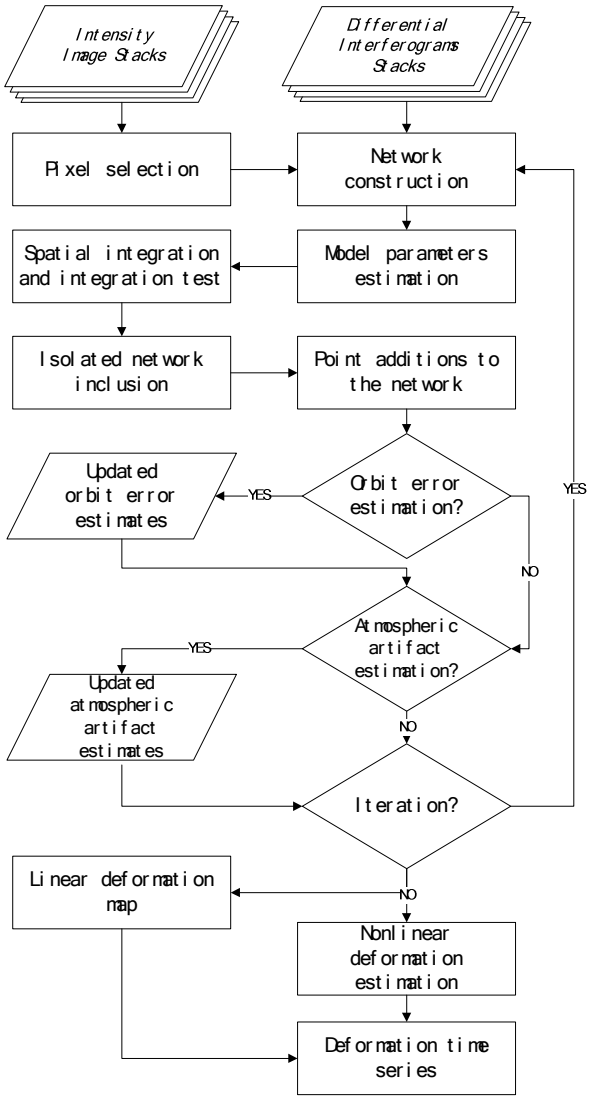

Figure 1 Block diagram of the GEOS-PSI estimation strategy.

The amplitude dispersion method (Ferretti et al. 2000, 2001) is used in this study to determine the stability of the phase in each pixel along the image stack. An empirical SAR calibration method based on the calibration methods of Casse (2004) and Kampes (2006) is developed to calibrate the SAR images. The calibration is carried out in two steps: (1) the amplitude observations of each SAR image are corrected using the calibration constant provided; (2) another calibration factor per image are calculated based on the modes of the potentially stable pixels (i.e. pixels with low amplitude dispersion index) of each image. Once the images are calibrated, the calculation for the amplitude dispersion index of each pixel can be performed. The amplitude dispersion index is used here to determine the reliability and quality of a stable pixel over time. The reference network is constructed using the reliable stable pixels (amplitude dispersion index < 0.25) based on the Delaunay triangulation network with a maximum arc length of 1.5km. The maximum arc length is chosen based on the expected spatial variation of the atmospheric and orbital errors (Blanco et al. 2008; Kampes and Adam 2003).

After the construction of reference network, the modelled parameters between pixels for each arc (i.e. displacement rate difference, DEM error difference and azimuth sub-pixel position difference) are estimated using the ILS estimator with LAMBDA method (described in Hanssen et al. 2001; Kampes and Hanssen 2004). The 'ensemble phase coherence', introduced by Ferretti et al. (2000, 2001), is used to evaluate the goodness-of-fit between the double-differenced phase observations of each arc fit and the modelled parameters difference. The arcs with absolute ensemble phase coherence lower than 0.75 are removed. After the estimation process for the parameter differences of all arcs in the reference network, the integration process and integration testing process, similar to the method used in adjusting a levelling network (described in Caspary 2000; Harvey 2006), are performed to calculate the absolute modelled parameters of each point.

The next step is to calculate the parameters of the isolated points (pixels not in the reference network). An adaptive estimation strategy has been developed in GEOS-PSI to calculate the parameters of the isolated points, consisting of two parts: adding an individual pixel into the reference network, and adding multiple pixels into the reference network. The parameters of each isolate pixel are estimated with respect to the pixels of the reference network within the spatial search window independently. Same integration and integration testing processes are performed to determine the absolute parameters of such pixel. If the pixel is rejected after the integration testing process, the same estimation process is carried out with a larger search window. The pixel is rejected if the size of the search window reaches the defined maximum search window size.

In order to maximises the number of isolated pixels to be added into the network. The isolated pixels are iteratively added into the network based on the pixel's stability and its distance from the reference network. This process is similar to the multi-layer process described by Blanco et al. (2006). In GOES-PSI, the isolated pixels are first sorted into different categories based on their reliability (determined by their amplitude dispersion index) and their distance from the reference network. The isolated pixels in category corresponding to higher reliability and shorter distance from the reference network are assigned with higher priority. The estimation process is carried out to the pixels with higher priority than the one with lower priority. The isolated pixel is added into the reference network if it passed the integration test. The rejected pixels (from the estimation process) are moved to the lower priority group. This estimation process is iteratively performed with the up-to-date reference network on the isolated pixels in the different categories until the last one is reached.

The orbital errors that are not correctly removed, especially in large baseline pairs, can introduce a spatial trend into the estimated modelled parameters (i.e. displacement rate, DEM error and azimuth sub-pixel position). In this study, the trends appeared in the displacement rate map, DEM error map and sub-pixel position map are removed if the gradient is larger than 1/4 of a fringe over the image scene, as they are unlikely to be the real signal. The unwrapped model phase for each pixel in the network in each interferograms is calculated based on the refined modelled parameters. The phase contributed by the atmospheric and orbital error is then addressed from the residual

phases (i.e. unwrapped modelled phase minus the differential interferometric phase). The residual phases for each interferogram are first unwrapped by the sparse MCF unwrapping algorithm (Costantini and Rosen 1999). To calculate the phase due orbital errors, least squares fitting is performed to estimate the linear trend in the unwrapped residual phases for each pair if the gradient of the trend is greater than ¼ of a fringe across the image scene. The atmospheric signal is estimated using the filtering operation discussed in PSInSAR approach (Ferretti et al. 2000, 2001), i.e. high-pass filtering in time followed by low-pass filtering in spatial. The atmospheric signal in the remaining pixels (not included in the network) can be estimated by TIN (bilinear) interpolation or kriging for extrapolation. In GEOS-PSI, the displacement, atmospheric and orbital error components are estimated iteratively as shown in Figure 1.

The final part of GEOS-PSI is to estimate the non-linear deformation component. To estimate the non-linear deformation component, low-pass filtering in both time and space is performed to the residual phases (calculated by removal of the phase contribution due to modelled parameters, atmospheric and orbit errors).

4. DATA USED

A total of forty nine C-band ENVISAT ASAR images acquired from 21 April 2003 to 6 September 2010 over Sydney were used in this study. The image acquired on 22 October 2007 was selected as the master image because of the relatively short perpendicular and temporal baseline corresponding to other images. Figure 2 shows the perpendicular baseline and the temporal baseline of all images with respect to the image acquired on 22 October 2007. Forty eight differential interferograms were generated with respect to the master image. In this study, an independently-derived DEM with a ground resolution of 25m, provided by the New South Wales Land and Property Management Authority, was used to remove topography phase from the interferograms.

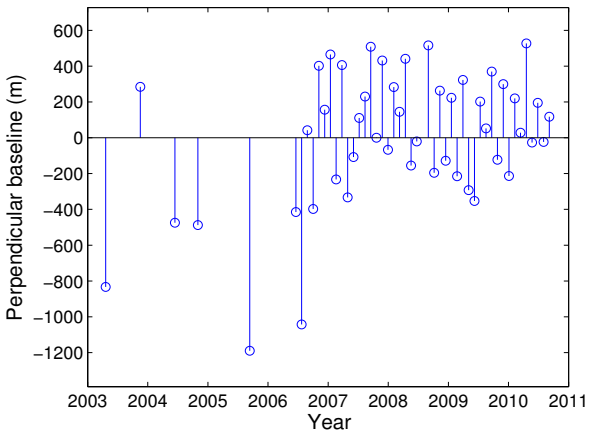

Figure 2. Baseline distribution of available ENVISAT ASAR data for Sydney area (Orbit direction: Descending; Imaging mode: I2; Tack: 402; Frame: 4290; Incidence angle: ~23°; Look direction: Right; Polarisation: VV).

5. RESULTS

In this study, the pixels with amplitude dispersion index less than 0.4 are selected for analysis where the one with amplitude dispersion index less 0.25 are used to construct the reference network. A total of 371675 stable pixels have been identified.

The linear displacement rate map (along radar line-of-sight (LOS) over Sydney is shown in Figure 3. The result demonstrates that the area of Sydney was relatively stable between 21 April 2003 and 6 September 2010 with deformation of the majority of persistent scatter points being within the range of -2 mm/yr to 2 mm/yr. The histogram in Figure 4 shows that the displacement rates of the pixel estimated are normally distributed with mean displacement rate of around 0 mm/yr and standard deviation of 1 mm/yr. The linear displacement rate map is overlaid with the water extraction bore and the boundary of Botany Sands Aquifer (Figure 5). No clear correlation between the groundwater extraction and the deformation pattern has been observed. The linear displacement rate map suggests that Sydney's south was experiencing a larger land movement. Displacement rate of up to -5.5 mm/yr has been observed in Woronora and Bonnet Bay, especially in area along the Woronora River.

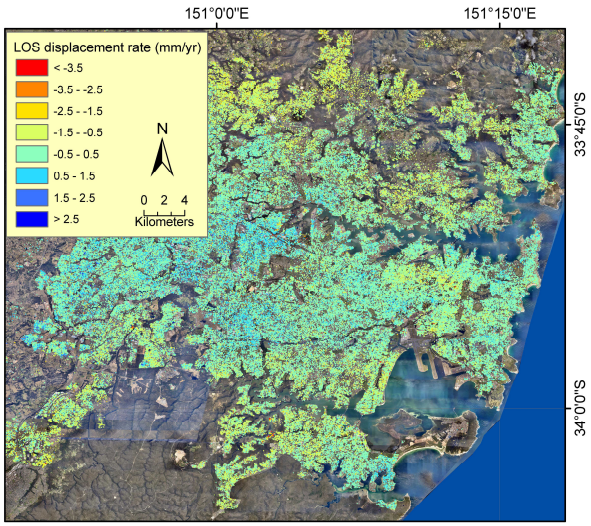

Figure 3. Sydney LOS displacement rate map.

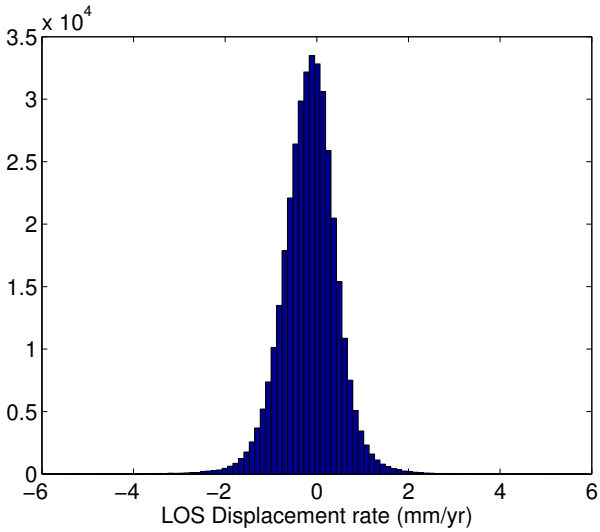

Figure 4. The distribution of displacement rates observed.

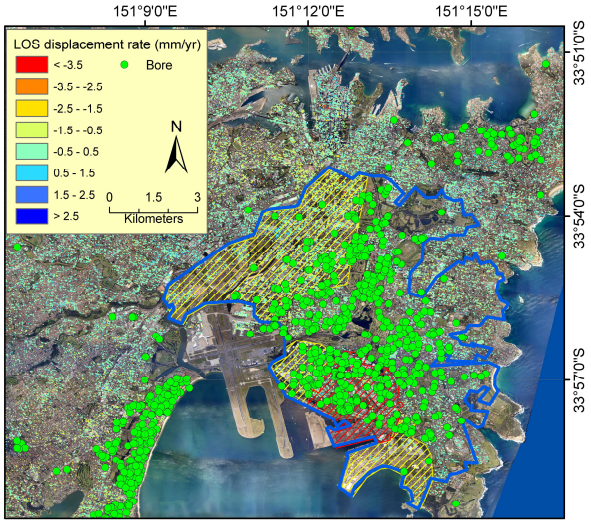

Figure 5. Sydney LOS displacement rate map overlaid with the water extraction bore and the boundary of Botany Sands Aquifer. The blue line represents the boundary of Botany Sands Aquifer.

6. CONCLUDING REMARKS

The GEOS-PSI estimation strategy has been presented in this study to map the land movement in Sydney, Australia. The linear displacement map was generated using 49 ENIVSAT ASAR images acquired from 2003 to 2010. The result shows that Sydney was reasonably stable in general. A normal distribution pattern has been observed from the displacement rate of the pixel estimated. There is no evidence for subsidence due to groundwater extraction in the Botany Sands Aquifer. Further investigation is necessary to understand the cause of the land deformation in Sydney's south.

ACKNOWLEDGEMENTS

This research work has been supported by the Cooperative Research Centre for Spatial Information through Project 4.09, whose activities are funded by the Australian Commonwealth's Cooperative Research Centres Programme. This study is also partially funded by a grant from the Ministry of Science and Technology of China under the China-Australia Special Fund for S&T Cooperation scheme.

The authors wish to thank the European Space Agency (ESA) for providing the ENVISAT ASAR data.

REFERENCES

P. Blanco, J. Mallorqui, S. Duque, & D. Monells, "The coherent pixels technique (CPT): An advanced DInSAR technique for nonlinear deformation monitoring," Pure and Applied Geophysics, vol 165, p.p. 1167-1193, 2008

P. Blanco, J. J. Mallorqui, S. Duque, & D. Navarrete, "Advances on DInSAR with ERS and ENVISAT data using the coherent pixels technique (CPT)," IGARSS 2006," Colorado, USA, p.p. 1898-1901, 31 July - 4 Aug, 2006

W. F. Caspary, "Concepts of Network and Deformation Analysis," Australia School of Geomatic Engineering, University of New South Wales, 183 p.p., 2000

B. N. Cassee, "Selection of Permanent Scatterer Candidates for Deformation Monitoring," Faculty of Civil Engineering and Geosciences, Delft University of Technology, The Netherlands, 93 p.p., 2004

M. Costantini, & P. A. Rosen, "A generalized phase unwrapping approach for sparse data," IGARSS 1999," Hamburg , Germany, p.p. 267-269, 28 June - 2 July, 1999

A. Ferretti, C. Prati, & F. Rocca, "Nonlinear subsidence rate estimation using permanent scatterers in differential SAR interferometry," IEEE Transactions on Geoscience and Remote Sensing, vol 38, p.p. 2202-2212, 2000

A. Ferretti, C. Prati, & F. Rocca, "Permanent scatterers in SAR interferometry," IEEE Transactions on Geoscience and Remote Sensing, vol 39, p.p. 8-20, 2001

L. Ge, A. H.-M. Ng, H. Wang, & C. Rizos, "Crustal deformation in Australia measured by satellite radar interferometry using ALOS/PALSAR imagery," Journal of Applied Geodesy, vol 3, p.p. 47-53, 2009

R. M. Goldstein, & C. L. Werner, "Radar interferogram filtering for geophysical applications," Geophysical Research Letters, vol 25, p.p. 4035–4038, 1998

R. F. Hanssen, "Radar Interferometry - Data Interpretation and Error Analysis," The Netherlands Kluwer Academic Publishers, 328 p.p., 2001

R. F. Hanssen, P. J. G. Teunissen, & P. Joosten, "Phase ambiguity resolution for stacked radar interferometric data," In, *Proceedings of International Symposium on Kinematic Systems in Geodesy, Geomatics and Navigation* (pp. 317-320). Banff, Canada2001

B. R. Harvey, "Practical Least Squares and Statistics for Surveyors," Australia School of Surveying & Spatial Information Systems, University of New South Wales, 332 p.p., 2006

J. Jankowski, & P. Beck, "Aquifer heterogeneity: hydrogeological and hydrochemical properties of the Botany Sands aquifer and their impact on contaminant transport," Australian Journal of Earth Sciences, vol 47, p.p. 45-64, 2000

B. Kampes, & R. F. Hanssen, "Ambiguity resolution for permanent scatterer interferometry," IEEE Transactions on Geoscience and Remote Sensing, vol 42, p.p. 2446-2453, 2004

B. M. Kampes, "Radar Interferometry: Persistent Scatterer Technique," Dordrecht Springer, 211 p.p., 2006

B. M. Kampes, & N. Adam, "Velocity field retrieval from long term coherent points in radar interferometric stacks," IGARSS 2003," Toulouse, France, p.p. 941-943 vol.942, 21-25 July, 2003

D. Massonnet, M. Rossi, C. Carmona, F. Adragna, G. Peltzer, K. Fiegl, & T. Rabaute, "The displacement field of the Landers earthquake mapped by radar interferometry," Nature, vol 364, p.p. 138-142, 1993

J. Mcdonald, "Dreamtime Superhighway: An Analysis of Sydney Basin Rock Art and Prehistoric Information Exchange," Canberra, Australia ANU E-Press, 380 p.p., 2008

A. H.-M. Ng, H. C. Chang, L. Ge, C. Rizos, & M. Omura, "Assessment of radar interferometry performance for ground subsidence monitoring due to underground mining," Earth, Planets and Space, vol 61, p.p. 733-745, 2009

S. Yun, P. Segall, & H. A. Zebker, "Constraints on magma chamber geometry at Sierra Negra volcano, Galapagos Islands, based on InSAR observations," Journal of Volcanology and Geothermal Research, vol 150, p.p. 232-243, 2006

K. Zhang, A. H.-M. Ng, L. Ge, Y. Dong, & C. Rizos, "Multi-path PALSAR interferometric observations of the 2008 magnitude 8.0 Wenchuan earthquake," International Journal of Remote Sensing, vol 31, p.p. 3449-3463, 2010